crystals

MDPI

Article

Pre-Recycling Material Analysis of NMC Lithium-Ion Battery Cells from Electric Vehicles

Anna Pražanová [1,*], Jan Kočí [1,2], Martin Havlík Míka [2], Dominik Pilnaj [1,3], Zbyněk Plachý [1] and Vaclav Knap [1]

[1] Department of Electrotechnology, Faculty of Electrical Engineering, Czech Technical University in Prague, Technická 1902/2, 166 27 Prague, Czech Republic
[2] Department of Glass and Ceramics, University of Chemistry and Technology, Technická 5, 166 28 Prague, Czech Republic
[3] Department of Environmental Chemistry and Technology, Faculty of Environment, Jan Evangelista Purkyně University in Ústí nad Labem, Pasteurova 3632/15, 400 96 Ústí nad Labem, Czech Republic
* Correspondence: anna.prazanova@cvut.cz

Abstract: Environmental concerns push for a reduction in greenhouse gas emissions and technologies with a low carbon footprint. In the transportation sector, this drives the transition toward electric vehicles (EVs), which are nowadays mainly based on lithium-ion batteries (LIBs). As the number of produced EVs is rapidly growing, a large amount of waste batteries is expected in the future. Recycling seems to be one of the most promising end-of-life (EOL) methods; it reduces raw material consumption in battery production and the environmental burden. Thus, this work introduces a comprehensive pre-recycling material characterization of waste nickel-manganese-cobalt (NMC) LIB cells from a fully electric battery electric vehicle (BEV), which represents a basis for cost-effective and environmentally friendly recycling focusing on the efficiency of the implemented technique. The composition of the NCM 622 battery cell was determined; it included a $LiNi_{0.6}Co_{0.2}Mn_{0.2}O_2$ spinel on a 15 µm Al-based current collector (cathode), a graphite layer on 60 µm copper foil (anode), 25 µm PE/PVDF polymer separator, and a $LiPF_6$ salt electrolyte with a 1:3 ratio in primary solvents DMC and DEC. The performed research was based on a series of X-ray, infrared (IR) measurements, gas chromatography–mass spectrometry (GC-MS), and inductively coupled plasma–optical emission spectrometry (ICP-OES) characterization of an aqueous solution with dissolved electrolytes. These results will be used in subsequent works devoted to optimizing the most suitable recycling technique considering the environmental and economic perspectives.

Keywords: lithium-ion battery (LIB); electric vehicle (EV); recycling process; waste battery; end-of-life treatment (EOL); material analysis

check for updates

Citation: Pražanová, A.; Kočí, J.; Míka, M.H.; Pilnaj, D.; Plachý, Z.; Knap, V. Pre-Recycling Material Analysis of NMC Lithium-Ion Battery Cells from Electric Vehicles. *Crystals* **2023**, *13*, 214. https://doi.org/10.3390/cryst13020214

Academic Editors: Xiaofei Yang, Fan Wu, Jingyu Lu and Deping Li

Received: 9 December 2022
Revised: 17 January 2023
Accepted: 19 January 2023
Published: 24 January 2023

Copyright: © 2023 by the authors. Licensee MDPI, Basel, Switzerland. This article is an open access article distributed under the terms and conditions of the Creative Commons Attribution (CC BY) license (https://creativecommons.org/licenses/by/4.0/).

1. Introduction

Nowadays, lithium-ion batteries (LIBs) represent a crucial energy storage technology [1,2]. They have found their place in various applications, from consumer portable electronics to complex stationary systems for energy storage, including smart grids and microgrids, particularly in the automotive industry [2–9]. LIBs are considered the most efficient technology for large-scale electrical power systems due to their high voltage and energy density, negligible memory effect, fast charging speed, and long cycle life [10,11]. Thus, they represent the heart of energy storage in present-day electric vehicles (EVs) [12,13].

More and more LIB applications are utilizing pouch cell design, an excellent solution for weight and cost reduction and optimizing packaging efficiency at the battery cell level [14,15]. Conductive foils, covered with active electrode materials, are divided with a separator and soaked with electrolytes. Several dozens of these cathode–separator–anode layers together represent one general battery cell, whose material composition is illustrated in Figure 1. The foil tabs are welded to the electrode and sealed to the aluminum (Al) pouch cover, carrying the positive and negative terminals [14,16–19].

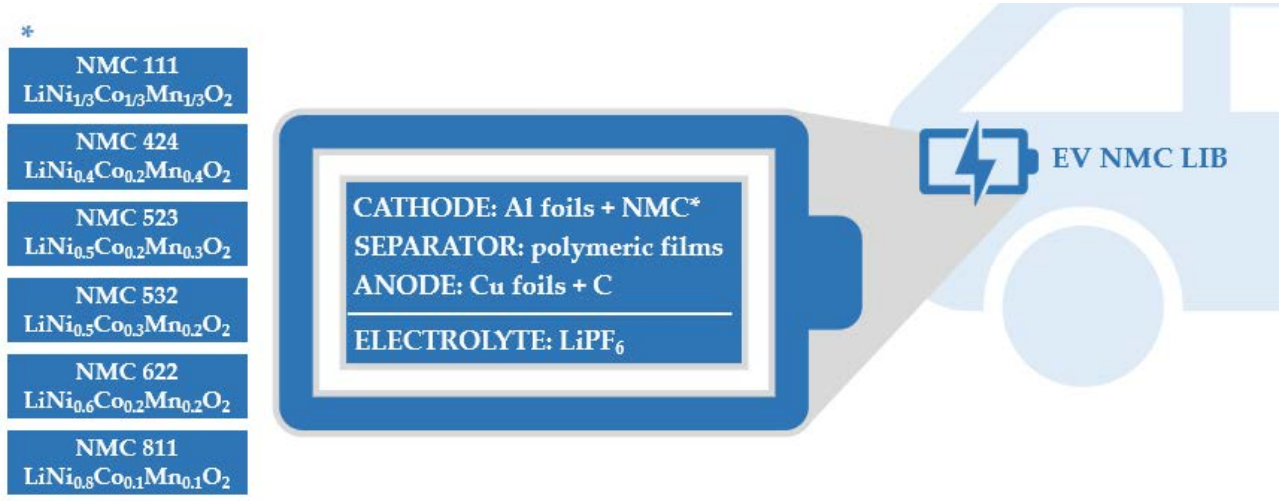


Figure 1. Composition of a general NMC LIB cell (* it complements individual NMC cell chemistries).

Lithium-nickel-manganese-cobalt-oxide ($LiNi_xMn_yCo_zO_2$) cathode material for LIBs, abbreviated as NMC, is today considered one of the most successful technologies [17,19,20]. It benefits from the properties of the blend of nickel (Ni), manganese (Mn), and cobalt (Co), where each metallic element plays a crucial role. The Ni furnishes the efficient capacity, the Co contributes to a good cycling life, and the Mn causes solid structural stability [20]. The NMC blend benefits of several varieties described according to the proportion of transition metal atoms. The basic formula of $LiNi_{1/3}Co_{1/3}Mn_{1/3}O_2$ consists of 33% Ni, 33% Mn, and 33% Co, typically referred to as 1-1-1 (NMC 111). The other typically used blends include $LiNi_{0.4}Co_{0.2}Mn_{0.4}O_2$ (NCM 424), $LiNi_{0.5}Co_{0.2}Mn_{0.3}O_2$ (NCM 523), $LiNi_{0.5}Co_{0.3}Mn_{0.2}O_2$ (NCM 532), $LiNi_{0.6}Co_{0.2}Mn_{0.2}O_2$ (NCM 622), and $LiNi_{0.8}Co_{0.1}Mn_{0.1}O_2$ (NCM 811) [17,20–22]. Aluminum (Al) has been widely used as a current collector for LIBs in recent years. It accounts for over 90% of the electric conductivity and approximately 90% of the cathode's mechanical strength in LIB cells [19,23].

The anode of the LIB cell is commonly created by graphite deposited on copper (Cu) foil. Graphite (C) is mainly used due to its reversible ability to position lithium (Li) ions between material layers of the cell. Similar properties are shown by other materials, such as activated carbon, carbon black, conductive additives, lithium titanate (LTO), silicon, or graphene [18,19,24].

Polyolefine (PO) membrane technology usually serves the LIB cell separator [25]. Depending on the manufacturing process, either polyethylene (PE) polymer and wax ("wet process") or PE or/and polypropylene (PP) polymer ("dry process") is used. These polymeric organic thin films can be additionally treated; for example, the polyvinylidene difluoride (PVDF) particles are used for obtaining strong polarity, stable electrochemical performance, and high thermal stability [25,26].

Nowadays, LIB manufacturers are focused on liquid electrolytes. A very common NMC LIB electrolyte is a 1-molar solution of highly conductive lithium hexafluorophosphate salt ($LiPF_6$) dissolved in various ratios of Ethylene Carbonate (EC):Diethyl Carbonate (DEC) and 2% Vinylene carbonate (VC) [27]. Although this electrolyte has excellent conductive properties, it dissociates into lithium fluoride (LiF) and phosphorus pentafluoride (PF_5), which reacts with moisture and forms hydrogen fluoride (HF) and phosphoryl fluoride (OPF_3) [25,28]. HF can lead to electrode material reactions that lose the power and capacity of the battery cell and represent high environmental and health risks due to the high acute toxicity, e.g., during end-of-life (EOL) processing [27,28].

The global targets of greenhouse gas emission reduction are rapidly driving the demand for alternative fuel vehicles with the benefit of a low carbon footprint [29–33]. Nevertheless, the still-increasing numbers of recently produced EVs bring new issues that must be solved; one of the most critical topics is the EOL processing of the ever-increasing

number of waste batteries [34,35]. Currently, the most prospective procedure is the recycling of waste batteries and the recovery of valuable and essential metals, such as Ni, Mn, Co, Li, Co, and Al [34,36–39].

Pyrometallurgy and hydrometallurgy are highly implemented techniques in recycling. The pyrometallurgical method is based on thermally treated batteries' physical and chemical transformation, with the process efficiency between 80–98.9% and 98–99.95% output purity. The hydrometallurgical process is created by chemical treatment, including acid or basic leaching, with an efficient process of around 76–98.2% and high-purity products between 96.5–99.7% [34,40–43]. The process efficiency entirely depends on the investment costs and equipment of the recycling plant [33,40]. Thus, the EU has responded to this critical automotive industry change and introduced new emission-free standards and regulations considering the real waste treatment solutions, determining the recycling efficiencies for LIBs to reach 65% by 2025 and 70% by 2030 [44].

Since there are many different EV LIBs on the market, it is necessary to understand the selected technology in its waste state before integrating the recycling process. Thus, this work contains a detailed pre-recycling material analysis of waste nickel-manganese-cobalt (NMC) LIB cells from a fully electric battery electric vehicle (BEV), which represents a basis for the effective recycling to meet the high EU requirements. Based on the performed X-ray and infrared (IR) spectra measurements, the cathode (Al foil and $LiNi_{0.6}Co_{0.2}Mn_{0.2}O_2$ spinel), anode (Cu foil and graphite layer), and separator (PE/PVDF thin film) materials were determined. Gas chromatography–mass spectrometry (GC-MS) and inductively coupled plasma–optical emission spectrometry (ICP-OES) were used for complete electrolyte characterization from the aqueous solution. The $LiPF_6$ salt with the main ratio of solvents 1:3 DMC:DEC was established for the cell. Moreover, the battery technology's valuable metals blend was set the closest to a $LiNi_{0.6}Co_{0.2}Mn_{0.2}O_2$ (NCM 622).

The content of this work is structured as follows: in Section 2, the detailed overview of used materials and methods is provided; in Section 3, the obtained results of NMC LIB cell material characterization are presented; in Section 4, the contribution of this work and its context of LIBs recycling in terms of future work is discussed; in Section 5, the main conclusions of this paper are pointed out.

2. Materials and Methods

The degradation process was determined using material analysis characterization on the waste nickel-manganese-cobalt (NMC) cells dismantled from a fully electric battery electric vehicle (BEV) module.

2.1. Materials

The waste NMC LIB pouch cells were used for laboratory testing, with each cell having a nominal voltage of 3.65 V and 78 Ah capacity. These cells were dismantled from the short-circuited battery module, commonly used in EV battery packs. The module consists of 24 cells in a 3P8S connection and a nominal voltage of 29.36 V and 6.85 kWh capacity.

2.2. Methods

This work used experimental methods for material analysis, such as X-ray diffraction (XRD) and fluorescence (XRF), infrared spectroscopy (IRS), light and electron microscopy, including mode of secondary electron (SE), and energy dispersive spectrometry (EDS). Moreover, one cell was opened and fully disassembled in 12 L of tap water to reduce the potential safety hazards associated with $LiFP_6$. The obtained aqueous solution was characterized in detail for determining the composition of the electrolyte using gas chromatography–mass spectrometry (GC-MS) and inductively coupled plasma–optical emission spectrometry (ICP-OES).

2.2.1. Material Analysis

This work is based on our previous work [45]. Moreover, a detailed analysis of electrodes, separator, and electrolyte from the light and electron microscopy, infrared spectroscopy (IRS), and spectrometry field was added. The performed methods used for the individual battery cell components' material characterizations are shown in the diagram according to Figure 2.

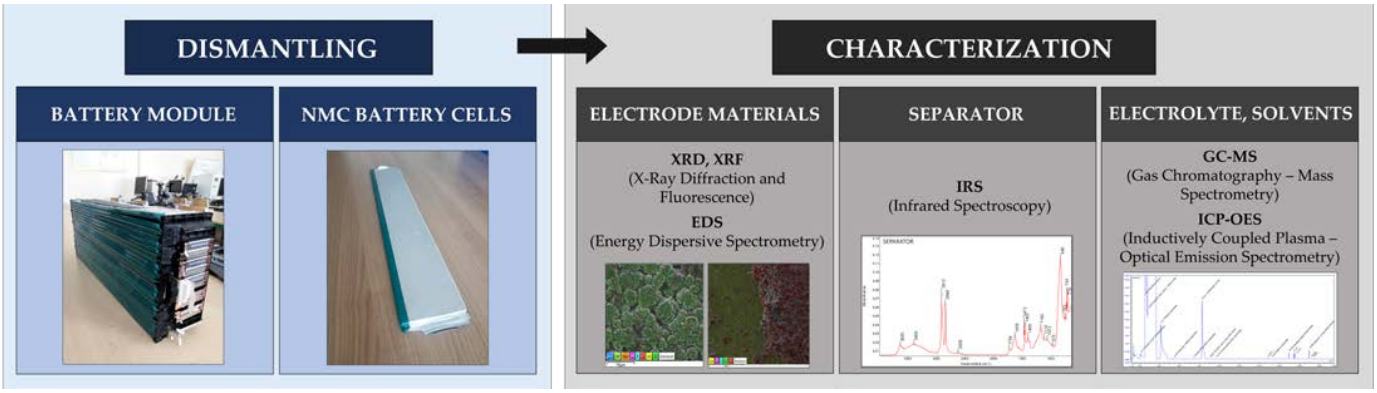


Figure 2. Material analysis methods used for battery cell characterization.

X-ray Diffraction and Fluorescence

The material of thin layers on metal sheets or a cell separator were analyzed using an X-ray fluorescence (XRF) with a Philips PANAlytical spectrometer and X-ray diffraction (XRD) with a Philips PANAlytical XPERT-PRO diffractometer.

Light and Electron Microscopy

Analyses of the thin films were carried out using an Olympus LEXT OLS5000 SAF confocal microscope at 5×, 10×, 20×, 50×, and 100× magnifications. A laser surface scanning mode was used for detailed illustration. Layer width measurements were performed in NIST Elements software.

Furthermore, the structures were characterized with a scanning electron microscope SEM TESCAN VEGA 3 LMU at an accelerating voltage of 10 kV and a working distance of 15 mm. It disposes of a ±0.1% error for each point of the relative error for a performed measurement. Surface morphologies were recorded in a mode of secondary electron (SE) and backscattered electrons (BSE) at a magnification of 300×, 500×, 2000×, and 3000×. In addition, a micro-X-ray elemental map was created using energy dispersive spectrometry (EDS).

Infrared Spectroscopy

The infrared (IR) ATR FTIR spectra were analyzed using a Thermo Scientific Nicolet 6700 spectrometer using a PIKE Technologies GladiATR reflective ATR extension with a diamond crystal. Spectra were recorded in the 4000–400 cm^{-1} region with a DLaTGS (deuterated L-alanine doped triglycine sulfate) detector with 4 cm^{-1} resolution, 64 scans, and Happ-Genzel apodization.

Gas Chromatography—Mass Spectrometry

Volatile solvents were characterized by a Thermo Fisher Scientific Trace 1310 GC coupled to a ISQ 7000 mass spectrometer. An autosampler TriPlus RSH used an SPME arrow (acrylate) extraction for the comprehensive identification of organic compounds present in the sample, and to estimate carbonate ratio headspace injection was performed. Both sample injection techniques preceded the incubation of a 1 mL sample at 80 °C for 30 min. GC separation ran on semi-standard non-polar column TG-5SILMS (30 m; 0.25 mm; 0.25 µm) with helium as a mobile phase (1.2 mL/min). The oven program started at 40 °C

held for 1 min followed by a 5 °C/min gradient up to 280 °C. A single quadrupole mass spectrometer was set to full scan acquisition with 5 Hz scan rate.

Inductively Coupled Plasma—Optical Emission Spectrometry

For quantitation of each element in aqueous solution containing electrolyte, Perkin Elmer Optima 8000 was set to monitor emission bands of Li (670.784 nm), Ni (231.604 nm), Mn (257.610 nm), Co (220.616 nm), Cu (327.393 nm), Al (396.153 nm), and P (213.617 nm). The samples were centrifuged and diluted 10× into 0.1% HNO_3, 100× if out of linear range.

3. Results

Pouch cells are made up of alternately layered cathode and anode materials, which are split by separators. Thus, firstly in this work, the cathode (on Al foil), anode (on Cu foil), and separator samples were analyzed. The tested NMC pouch cell consists of 36 spinel-separator-graphite cells. The analyzed layer composition with the determined materials' thicknesses is illustrated in the structure scheme in Figure 3. Within these characterization measurements, one side of each metal foil was covered by a visually pure material layer, and on the second side a layer was deposited containing remains of the separator, which were confirmed by energy dispersive spectroscopy.

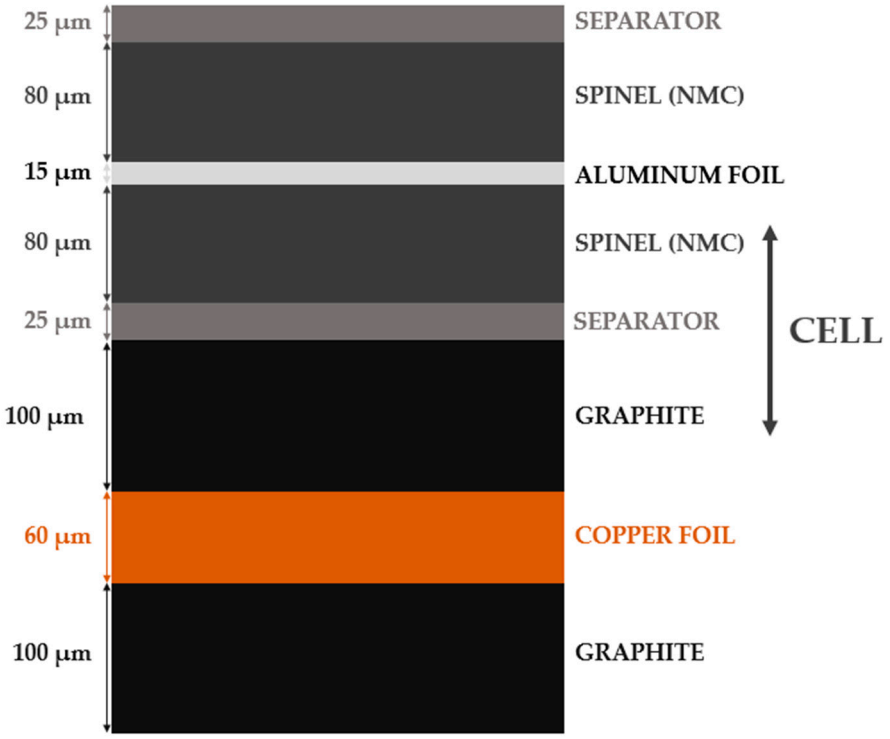


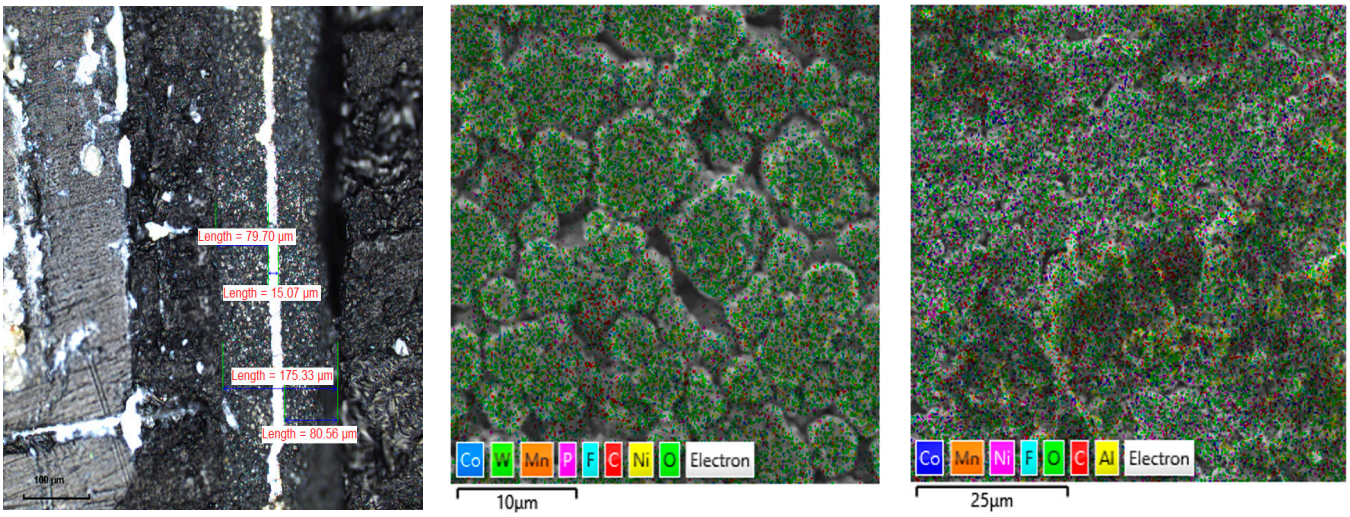
Figure 3. Scheme of the analyzed NMC battery cell structure.

The XRD and XRF methods supplemented with EDS element maps were used for the determination of the stoichiometric composition of the materials; the IR was performed for the separator analysis. ICP-OES, and GC-MS were performed for the analysis of the dissolved electrolyte in an aqueous solution. The results, including average thickness and experimental method for the individual material, are shown in Table 1.

The cathode active material layer is thick, approximately 175 µm; it is formed by a 15 um Al foil and an 80 µm spinel layer adjoined on each side. A detail of the material thickness is shown in Figure 4a.

Table 1. The material composition of the individual components of the battery cell; average thicknesses of individual material layers; methods used to characterize the material composition.

Battery Cell Component	Material Composition	Material Thickness	Analysis Method
Cathode	Al foil $LiNi_{0.6}Mn_{0.2}Co_{0.2}O_2$	15 µm 80 µm in one layer	XRD, XRF, EDS
Anode	Cu foil carbon	60 µm 100 µm in one layer	XRD, XRF, EDS
Separator	PE/PVDF	25 µm	IR
Electrolyte	$LiPF_6$	-	ICP-OES
Solvents	Carbonates, FB	-	GC-MS



(**a**) (**b**) (**c**)

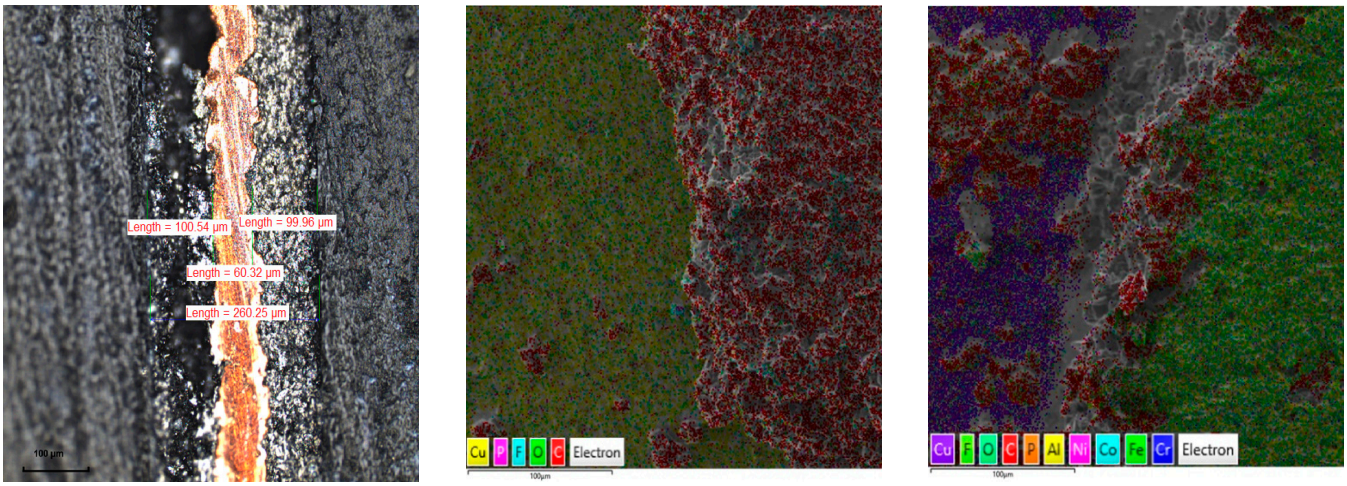
Figure 4. The cathode of the battery cell: (**a**) cross-section of a spinel double layer on Al foil with an illustration of materials layer thickness; (**b**) EDS element map of visually pure side of spinel layer; (**c**) EDS element map of spinel layer with separator residues.

The surface of the cathode material samples was X-rayed in EDS; the elemental maps for the visually pure spinel layer and the layer with separator residues are shown in Figure 4b,c. Based on the results shown in Table 2 and the XRF measurement, with the ratio between Ni:Mn:Co in 55:24:20 mol.%, the NMC 622 blend was determined for the spherical spinel particles of the tested battery cell. The presence of tungsten (W) was confirmed by both EDS and XRF analysis. It is probably an additive in the form of, e.g., tungsten trioxide (WO_3), to improve the cathode materials' electron conductivity and redox reaction kinetics as illustrated by Meng et al. [46] or Gan et al. [47].

Table 2. Results of the EDS element map for the battery cathode.

Element	Visually Pure Layer		Layer with Separator Residues	
	Weight (wt.%)	σ (wt.%)	Weight (wt.%)	σ (wt.%)
Ni	28.0	2.7	23.1	2.2
O	23.7	1.1	21.7	0.8
F	16.4	0.8	16.7	0.7
C	10.9	0.7	15.0	0.7
Mn	8.5	0.9	7.4	0.7
Co	7.3	1.6	7.8	1.3
W	3.8	0.5	1.5	0.3
P	1.3	0.2	0.6	0.1
Al	-		6.1	0.3

The entire carbon bilayer deposited on a Cu (anode) is around 100 µm thicker than the layer of cathode materials (it measures 260 µm in total). The Cu foil has an average of 60 µm, with each spinel layer 100 µm thick. A detail of the active material thickness is shown in Figure 5a.



(**a**) (**b**) (**c**)

Figure 5. The anode of the battery cell: (**a**) cross-section of a graphite double layer on Cu foil with an illustration of materials layer thickness; (**b**) EDS element map of visually pure layer; (**c**) EDS element map of graphite layer with separator residues.

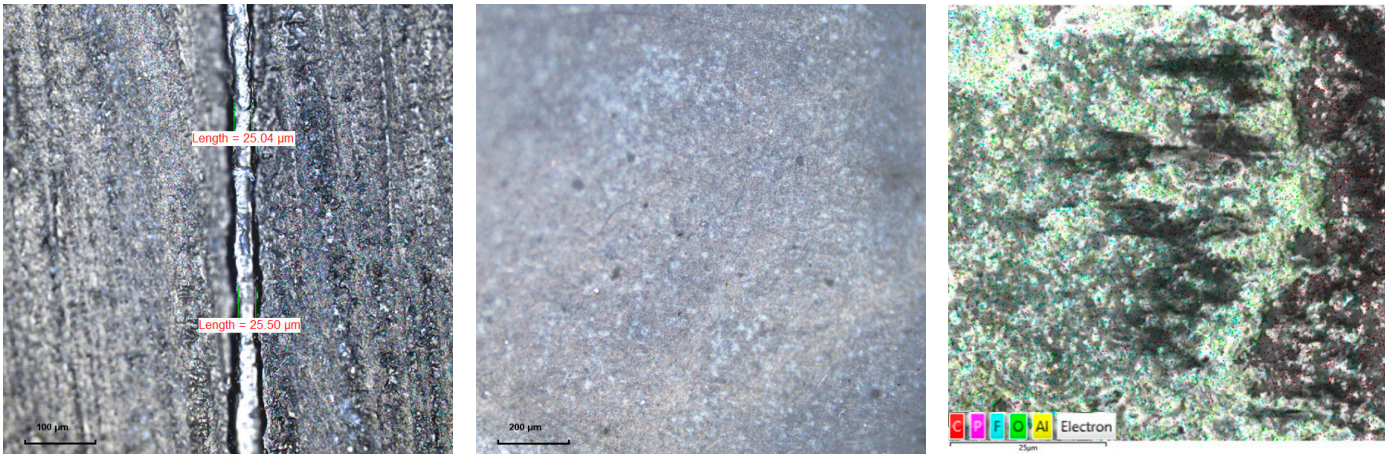
The sample surface of anode materials was X-rayed in EDS mode; the elemental maps for the visually pure layer and spinel with separator residues are shown in Figure 5b,c, respectively. The elemental analysis shown in Table 3 detected electrolyte residues (containing F and P) and confirmed the presence of a separator (based on Al). The material layer was determined to be >90% pure graphite based on the results of XRF analysis.

Table 3. Results of the EDS element map for the battery anode.

Element	Visually Pure Layer		Layer with Separator Residues	
	Weight (wt.%)	σ (wt.%)	Weight (wt.%)	σ (wt.%)
C	48.0	0.6	35.8	0.7
Cu	39.1	0.6	23.0	0.4
O	6.0	0.2	14.1	0.3
F	4.3	0.2	10.4	0.2
P	1.1	0.1	2.6	0.1
Al	-		12.9	0.1

The battery separator macroscopically appeared as a rigid, flexible polymer thin film of an approximate thickness of 25 µm. A detail of the separator cross-section and an optical image of the structure are shown in Figure 6a and b, respectively.

Due to the separator samples' high fluorescence, it was impossible to use Raman spectroscopy to determine their composition. Therefore, the separator's IR spectrum was measured, as shown in Figure 7.



(**a**) (**b**) (**c**)

Figure 6. The separator of the battery cell: (**a**) cross-section with an illustration of material layer thickness; (**b**) optical image from a confocal microscope; (**c**) EDS element map.

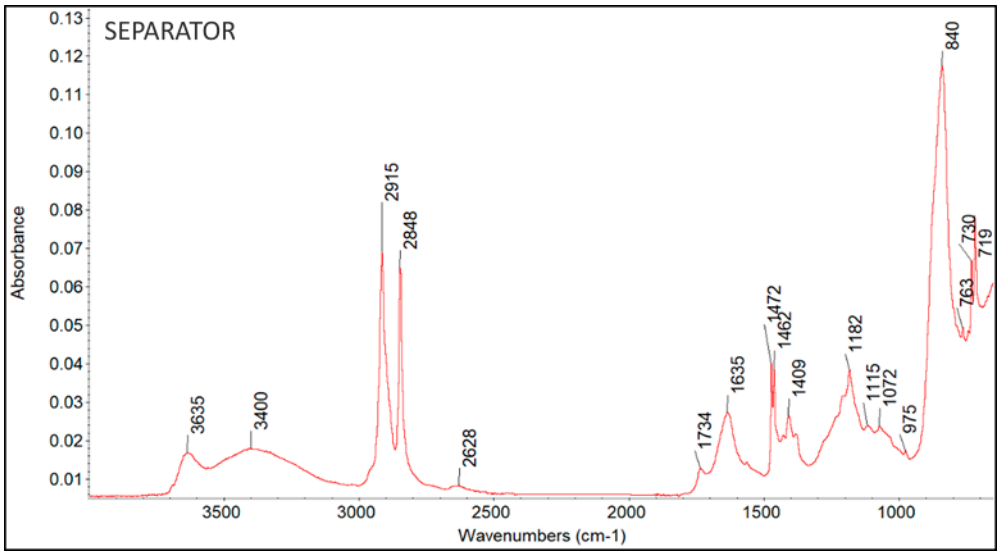


Figure 7. IR spectrum of the separator.

To interpret the spectrum, polyethylene film (PE) was used as a reference material and was measured under the same conditions (Figure 8). Comparing these two spectra concluded that the absorption bands at 2915, 2848, 1472, 1462, 730, and 719 cm^{-1} correspond to the polyethylene polymer.

To interpret the whole spectrum, individual absorption bands were identified using reference materials, spectrum libraries, and the available literature. The main component of the separator material was determined as the PE/PVDF polymer. The absorption bands at 1409, 1182, 1072, and 840 cm^{-1} correspond to the polyvinylidene fluoride. The other absorption bands were assigned to hexafluorophosphate $[PF_6]^-$, aluminum oxide (Al_2O_3), and residual carbon. The elements of all materials were confirmed by elemental analysis,

and the identified materials correspond with previously published results, where the PE separator with surface coating modification is commonly used for LIBs due to its high thermal dimensional stability and excellent electrolyte wettability. The properties of the same type of separator (PE separator coated by PVDF particles) were discussed in work by Wang et al. [48].

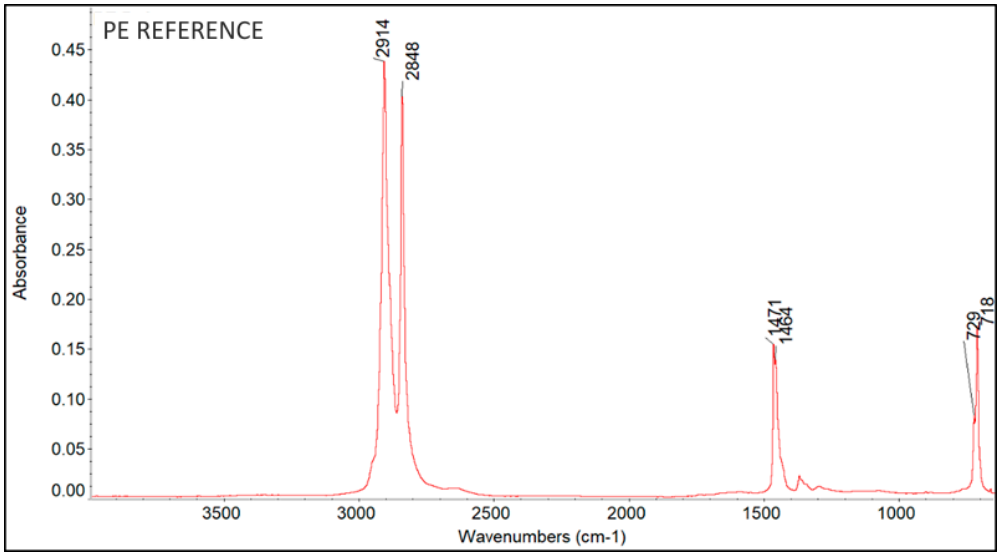


Figure 8. IR spectrum of the polyethylene reference foil PE Reference.

These results support the presence of C, Al, and F atoms detected by the EDS element map, of which the results are shown in Figure 6c and in Table 4.

Table 4. Results of the EDS element map for the battery separator.

Element	Separator	
	Weight (wt.%)	**σ (wt.%)**
F	31.9	0.5
C	29.2	0.7
O	19.8	0.4
Al	15.7	0.3
P	3.5	0.2

Based on a performed characterization, lithium hexafluorophosphate ($LiPF_6$) electrolyte residues, containing F and P, were determined on both electrodes using EDS spectrometry mode and on a battery separator by IR spectra measurement.

Regardless, the electrolyte composition was analyzed in the second part of this work. The electrolyte solvents from the aqueous solution were analyzed in detail using GC-MS and ICP-OES. The cell was cut open in water, disassembled from the Al package, and hand-crushed, and then the coarse solid parts were removed from the solution. The results of the analysis are shown in Table 5.

Table 5. Electrolyte and electrode dissolution in aqueous solution.

Concentration (mg/L)	Al	Co	Cu	Li	Mn	Ni	P
Blank	<LOQ	<LOQ	1.6	0.1	<LOQ	<LOQ	1.7
Cell opening (time: 0:00)	<LOQ	<LOQ	2.0	12.5	<LOQ	<LOQ	764.8
Cell disassembly (time: 0:30)	2.5	0.1	18.8	110.5	0.3	0.4	4 316.8
Cell crushing (time: 0:45)	3.3	0.1	18.0	106.4	0.4	0.5	4 139.8
Removal of solids (time: 1:00)	8.6	0.2	17.6	133.1	0.8	1.1	4 501.1
mg/one cell	103.0	3.0	210.8	1 597.6	9.5	13.8	54 012.8

LOQ = limit of quantification.

A trace amount of Co, Mn, and Ni was dissolved, whereas Al and Cu were released from the solid phase in a slightly higher amount. The most abundant element observed was phosphorus (P), most likely phosphates. The amount of Li observed is significantly lower than P, probably due to the formation of insoluble lithium salts.

The most abundant solvent identified according to the chromatogram illustrated in Figure 9 was methyl ethyl carbonate (EMC), followed by its dimethyl and diethyl esters; a significant amount of fluorobenzene (C_6H_5F) was observed.

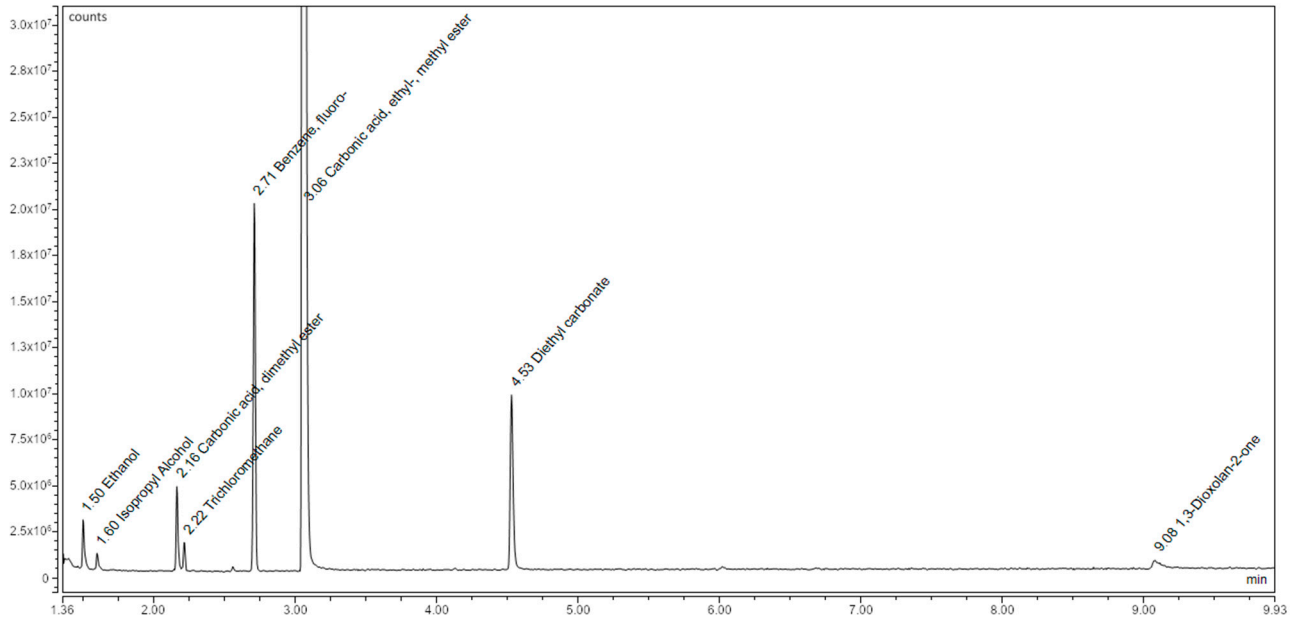


Figure 9. Chromatogram of headspace injection for estimation of carbonate ratio and identification of major organic solvents.

Solid-phase microextraction (SPME) revealed trace amounts of other carbonic acid esters with various carbon chain lengths, as visible in Figure 10. All these compounds have high vapor pressure and migrate into the air.

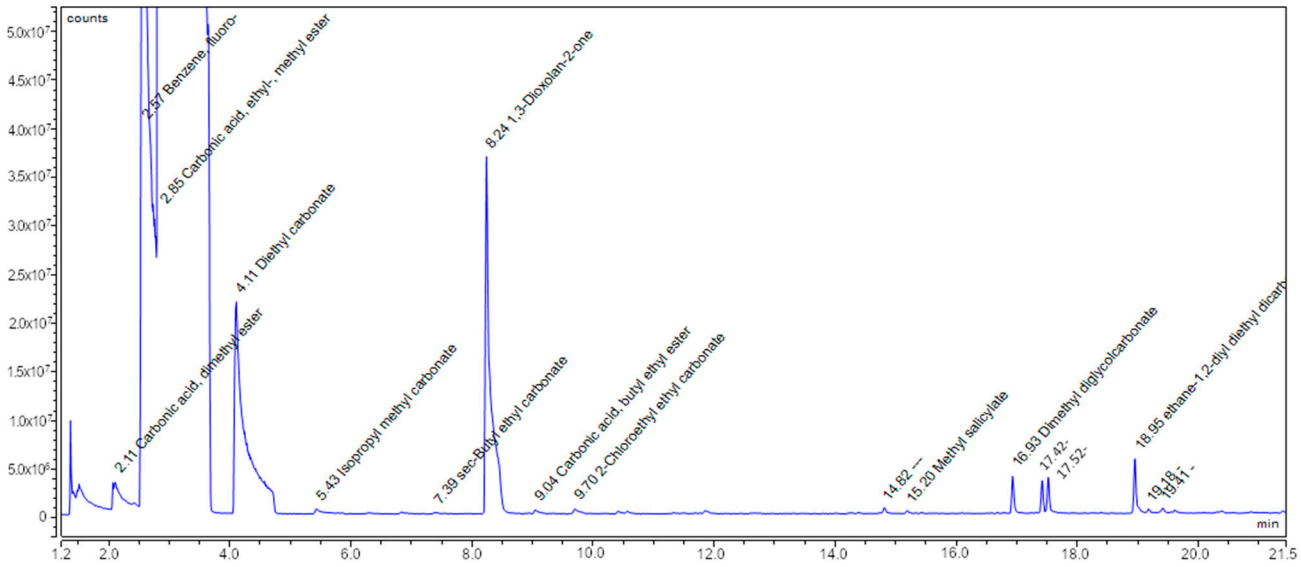


Figure 10. SPME extraction of volatile solvents from aqueous solution, further identification of trace carbonates.

The ratio for the primarily used solvents for $LiPF_6$ salt electrolyte, dimethyl carbonate (DMC), and diethyl carbonate (DEC), was established as 1:3. These results were determined for the waste NMC cell based on the electrolyte release into an aqueous solution.

Based on the experimental results of this work, LIB NMC pouch cells consisting of 36 spinel-separator-graphite cells in total were characterized in detail. According to the performed analyses, including XRD, XRF, EDS, and IR measurements, the cathode of the battery cell is created by the 15 µm Al-based current collector, which is covered from both sides by the 80 µm NMC 622 spinel. The battery anode is made up of 60 µm Cu foil, with graphite layers deposited on both sides with a >90% purity. The cathode and anode materials are split by a separator based on PE/PVDF polymers, ensuring high thermal dimensional stability and excellent electrolyte wettability. The battery cell electrolyte was determined based on a $LiPF_6$ salt with a 1:3 ratio in primary solvents DMC and DEC with MEC being the main component; the characterization was set up by GC-MS and ICP-OES measurements of an aqueous solution containing released electrolyte and active material residues.

4. Discussion

This work represents an important step in the EOL processing of NMC LIB technology, as it characterizes in detail the material composition of the waste cell. During operation, the active materials of the electrodes, current collectors, separator, and electrolyte degrade, i.e., change their capabilities. Therefore, it is necessary to characterize the state of cells at the beginning and end of their life to precisely define the input products of recycling processing.

The results of this work create a basis for future work, as shown in Figure 11. Detailed material characterization of the NMC technology will be used to optimize the individual steps of currently used recycling techniques, focusing on achieving the highest possible process efficiency and purity of recovered materials whilst considering the investment and operating costs. Moreover, the environmental impact based on the performed analysis results will be described, including wastewater treatment (containing toxic electrolyte residues) or emissions generated during high-temperature processing. The work will also focus on recovery from secondary processes, e.g., wastewater, which would directly support the principle of lossless recycling.

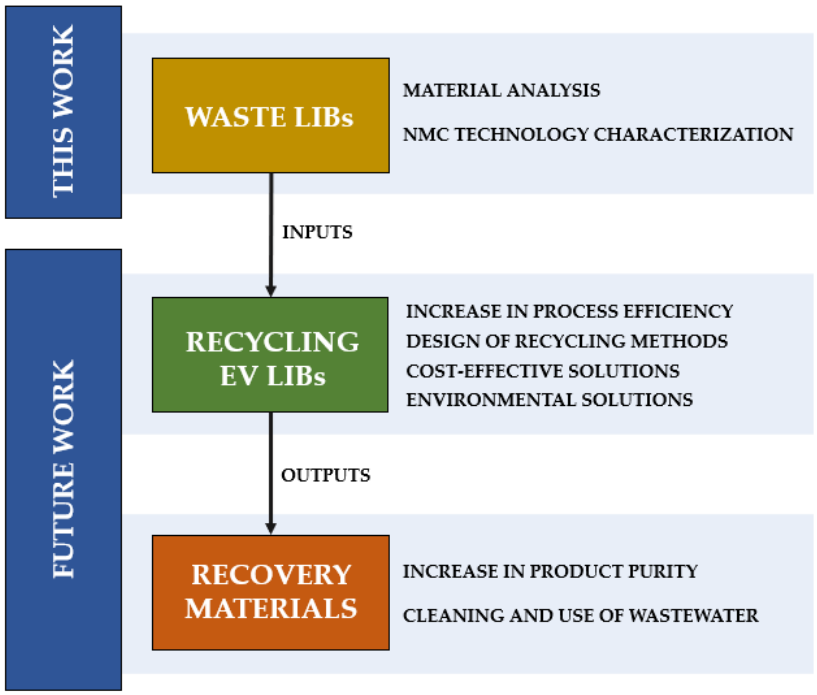


Figure 11. Inclusion of this work in the context of LIBs recycling and follow-up work.

The performed analysis was carried out to characterize waste battery cells' material state before recycling. Thus, fully discharged (short-circuited) cells were used for evaluation; this could have degraded and changed the structure of the materials. Thus, the obtained material analysis might not be completely valid for a fresh cell.

Although the market for LIBs is still growing, understanding the currently widely used technologies is a necessary basis that will lead to the successful compliance with the high EU requirements for EOL processing and faster adaptation when processing new technologies.

5. Conclusions

This work performed a detailed pre-recycling material analysis of the LIB NMC cell, commonly used in a BEV. Results of the presented battery cell material composition can be used as a basis for better understanding the degradation mechanism of NMC technology, process modeling, and for implementing ecologically and economically beneficial EOL processing, including high-efficiency recycling.

Detailed characterization results of LIB NMC cells, including analysis of the active electrode materials, separator, and electrolyte composition, were presented in this paper. The results will be followed up in subsequent works. Determining the exact material ratios of the waste battery pouch cells, established as NMC 622 (based on $LiNi_{0.6}Co_{0.2}Mn_{0.2}O_2$ spinel), will be used to elucidate the cell's degradation mechanisms, focusing on electrode material changes and electrolyte decomposition, compared with analyses of the new cell technology being tested.

Moreover, this work represents a necessary step that precedes recycling the entire battery cell. The results will be used in the follow-up work, devoted to selecting and optimizing the most suitable recycling technique focusing on recovering the highest possible proportion of crucial materials and their sufficient quality when reused in EV LIB cell production. Moreover, in terms of recycling, the explicit materials characterization will be part of the process modeling, considering the economic and environmental impacts of implementing recovery techniques.

Author Contributions: Conceptualization, A.P. and J.K.; methodology, A.P.; formal analysis, J.K.; investigation, J.K. and M.H.M.; resources, A.P., J.K., M.H.M., Z.P. and D.P.; data curation, A.P. and J.K.; writing—original draft preparation, A.P.; writing—review and editing, A.P., M.H.M., J.K., D.P. and V.K.; supervision, M.H.M. and V.K.; project administration, A.P. All authors have read and agreed to the published version of the manuscript.

Funding: This research received no external funding.

Data Availability Statement: The measured data was presented in this publication in figures and tables; thus, no dataset sharing was stated.

Conflicts of Interest: The authors declare no conflict of interest.

References

1. Armand, M.; Axmann, P.; Bresser, D.; Copley, M.; Edström, K.; Ekberg, C.; Guyomard, D.; Lestriez, B.; Novák, P.; Petranikova, M.; et al. Lithium-ion batteries—Current state of the art and anticipated developments. *J. Power Sources* **2020**, *479*, 228708. [CrossRef]
2. Chen, H.; Cong, T.N.; Yang, W.; Tan, C.; Li, Y.; Ding, Y. Progress in electrical energy storage system: A critical review. *Prog. Nat. Sci.* **2009**, *19*, 291–312. [CrossRef]
3. Ambrose, H.; Gershenson, D.; Gershenson, A.; Kammen, D. Driving rural energy access: A second-life application for electric-vehicle batteries. *Environ. Res. Lett.* **2014**, *9*, 094004. [CrossRef]
4. Chen, W.; Liang, J.; Yang, Z.; Li, G. A Review of Lithium-Ion Battery for Electric Vehicle Applications and Beyond. *Energy Procedia* **2019**, *158*, 4363–4368. [CrossRef]
5. Chen, T.; Jin, Y.; Lv, H.; Yang, A.; Liu, M.; Chen, B.; Xie, Y.; Chen, Q. Applications of Lithium-Ion Batteries in Grid-Scale Energy Storage Systems. *Trans. Tianjin Univ.* **2020**, *26*, 208–217. [CrossRef]
6. Knap, V.; Kjelgaard Vestergaard, L.; Gismero, A.; Stroe, D.-I.; Knap, V.; Vestergaard, L.; Gismero, A. In Proceedings of the 71st International Astronautical Congress, Dubai, United Arab Emirates, 12–16 October 2020.
7. Fallahifar, R.; Kalantar, M. Optimal planning of lithium ion battery energy storage for microgrid applications: Considering capacity degradation. *J. Energy Storage* **2023**, *57*, 106103. [CrossRef]
8. González, I.; Calderón, A.J.; Folgado, F.J. IoT real time system for monitoring lithium-ion battery long-term operation in microgrids. *J. Energy Storage* **2022**, *51*, 104596. [CrossRef]
9. Wei, Y.; Wang, S.; Han, X.; Lu, L.; Li, W.; Zhang, F.; Ouyang, M. Toward more realistic microgrid optimization: Experiment and high-efficient model of Li-ion battery degradation under dynamic conditions. *eTransportation* **2022**, *14*, 100200. [CrossRef]
10. Tomaszewska, A.; Chu, Z.; Feng, X.; O'Kane, S.; Liu, X.; Chen, J.; Ji, C.; Endler, E.; Li, R.; Liu, L.; et al. Lithium-ion battery fast charging: A review. *eTransportation* **2019**, *1*, 100011. [CrossRef]
11. Kim, T.; Song, W.; Son, D.-Y.; Ono, L.K.; Qi, Y. Lithium-ion batteries: Outlook on present, future, and hybridized technologies. *J. Mater. Chem. A* **2019**, *7*, 2942–2964. [CrossRef]
12. Bonsu, N.O. Towards a circular and low-carbon economy: Insights from the transitioning to electric vehicles and net zero economy. *J. Clean. Prod.* **2020**, *256*, 120659. [CrossRef]
13. Skeete, J.-P.; Wells, P.; Dong, X.; Heidrich, O.; Harper, G. Beyond the EVent horizon: Battery waste, recycling, and sustainability in the United Kingdom electric vehicle transition. *Energy Res. Soc. Sci.* **2020**, *69*, 101581. [CrossRef]
14. Kim, J.-S.; Lee, D.-C.; Lee, J.-J.; Kim, C.-W. Optimization of Lithium-Ion Battery Pouch Cell for Maximization of Energy Density while Preventing Internal Short Circuit Caused by Separator Failure under Crush Load. *J. Electrochem. Soc.* **2021**, *168*, 030536. [CrossRef]
15. Löbberding, H.; Wessel, S.; Offermanns, C.; Kehrer, M.; Rother, J.; Heimes, H.; Kampker, A. From Cell to Battery System in BEVs: Analysis of System Packing Efficiency and Cell Types. *World Electr. Veh. J.* **2020**, *11*, 77. [CrossRef]
16. Halimah, P.N.; Budiman, B.A.; Sambegoro, P.L. Mechanical properties of pouch battery constituents. *AIP Conf. Proc.* **2020**, *2217*, 030097. [CrossRef]
17. Günter, F.J.; Wassiliadis, N. State of the Art of Lithium-Ion Pouch Cells in Automotive Applications: Cell Teardown and Characterization. *J. Electrochem. Soc.* **2022**, *169*, 030515. [CrossRef]
18. Battery University Homepage. Available online: https://batteryuniversity.com/ (accessed on 5 December 2022).
19. Sustainable Commodities and Supply Chain Solutions | Targray. Available online: https://www.targray.com/ (accessed on 5 December 2022).
20. Chen, S.; Zhang, X.; Xia, M.; Wei, K.; Zhang, L.; Zhang, X.; Cui, Y.; Shu, J. Issues and challenges of layered lithium nickel cobalt manganese oxides for lithium-ion batteries. *J. Electroanal. Chem.* **2021**, *895*, 115412. [CrossRef]
21. Xuan, W.; Otsuki, A.; Chagnes, A. Investigation of the leaching mechanism of NMC 811 ($LiNi_{0.8}Mn_{0.1}Co_{0.1}O_2$) by hydrochloric acid for recycling lithium ion battery cathodes. *RSC Adv.* **2019**, *9*, 38612–38618. [CrossRef] [PubMed]
22. Chen, Z.; Wang, Z.; Kim, G.T.; Yang, G.; Wang, H.; Wang, X.; Huang, Y.; Passerini, S.; Shen, Z. Enhancing the Electrochemical Performance of $LiNi_{0.4}Co_{0.2}Mn_{0.4}O_2$ by V_2O_5/LiV_3O_8 Coating. *ACS Appl. Mater. Interfaces* **2019**, *11*, 26994–27003. [CrossRef] [PubMed]

23. Theivaprakasam, S.; Girard, G.; Howlett, P.; Forsyth, M.; Mitra, S.; MacFarlane, D. Passivation behaviour of aluminium current collector in ionic liquid alkyl carbonate (hybrid) electrolytes. *Npj Mater. Degrad.* **2018**, *2*, 13. [CrossRef]
24. Holze, R. Anodes—Materials for negative electrodes in electrochemical energy technology. *AIP Conf. Proc.* **2014**, *1597*, 44–65. [CrossRef]
25. Weber, C.J.; Geiger, S.; Falusi, S.; Roth, M. Material review of Li ion battery separators. *AIP Conf. Proc.* **2014**, *1597*, 66–81. [CrossRef]
26. Liu, R.; Yuan, B.; Zhong, S.; Liu, J.; Dong, L.; Ji, Y.; Dong, Y.; Yang, C.; He, W. Poly(vinylidene fluoride) separators for next-generation lithium based batteries. *Nano Sel.* **2021**, *2*, 2308–2345. [CrossRef]
27. Zackrisson, M.; Schellenberger, S. *Toxicity of Lithium Ion Battery Chemicals—Overview with Focus on Recycling*; Rise: Borås, Sweden, 2020.
28. Balbuena, P.B. Electrolyte materials—Issues and challenges. *AIP Conf. Proc.* **2014**, *1597*, 82. [CrossRef]
29. Elgowainy, A.; Burnham, A.; Wang, M.; Molburg, J.; Rousseau, A. Well-to-Wheels Energy Use and Greenhouse Gas Emissions Analysis of Plug-in Hybrid Electric Vehicles Energy Systems Division. *Cent. Transp. Res. Energy Syst. Div. Argonne Natl. Lab.* **2009**, *2*, 627–644.
30. McLaren, J.; Miller, J.; O'Shaughnessy, E.; Wood, E.; Shapiro, E. CO2 emissions associated with electric vehicle charging: The impact of electricity generation mix, charging infrastructure availability and vehicle type. *Electr. J.* **2016**, *29*, 72–88. [CrossRef]
31. Tang, Y.; Cockerill, T.T.; Pimm, A.J.; Yuan, X. Reducing the life cycl4e environmental impact of electric vehicles through emissions-responsive charging. *iScience* **2021**, *24*, 103499. [CrossRef]
32. Xu, B.; Sharif, A.; Shahbaz, M.; Dong, K. Have electric vehicles effectively addressed CO2 emissions? Analysis of eight leading countries using quantile-on-quantile regression approach. *Sustain. Prod. Consum.* **2021**, *27*, 1205–1214. [CrossRef]
33. Pražanová, A.; Knap, V.; Stroe, D.-I. Literature Review, Recycling of Lithium-Ion Batteries from Electric Vehicles, Part II: Environmental and Economic Perspective. *Energies* **2022**, *15*, 7356. [CrossRef]
34. Chen, M.; Ma, X.; Chen, B.; Arsenault, R.; Karlson, P.; Simon, N.; Wang, Y. Recycling End-of-Life Electric Vehicle Lithium-Ion Batteries. *Joule* **2019**, *3*, 2622–2646. [CrossRef]
35. Forsgren, C. Lithium-Ion Batteries, How to Generate Value Out of End of Life Mobile Units. *Miner. Met. Mater. Ser.* **2019**, 261–263. [CrossRef]
36. MarketsandMarkets Preview: Lithium-ion Battery Recycling Market Global Forecast to 2030 | MarketsandMarkets. Available online: https://www.marketsandmarkets.com/Market-Reports/lithium-ion-battery-recycling-market-153488928.html (accessed on 19 September 2021).
37. Gu, S.; Zhang, L.; Fu, B.; Ahn, J.W.; Wang, X. Recycling of mixed lithium-ion battery cathode materials with spent lead-acid battery electrolyte with the assistance of thermodynamic simulations. *J. Clean. Prod.* **2020**, *266*, 121827. [CrossRef]
38. Park, K.; Yu, J.; Coyle, J.; Dai, Q.; Frisco, S.; Zhou, M.; Burrell, A. Direct Cathode Recycling of End-Of-Life Li-Ion Batteries Enabled by Redox Mediation. *ACS Sustain. Chem. Eng.* **2021**, *9*, 8214–8221. [CrossRef]
39. Natarajan, S.; Aravindan, V. Recycling Strategies for Spent Li-Ion Battery Mixed Cathodes. *ACS Energy Lett.* **2018**, *3*, 2101–2103. [CrossRef]
40. Pražanová, A.; Knap, V.; Stroe, D.-I. Literature Review, Recycling of Lithium-Ion Batteries from Electric Vehicles, Part I: Recycling Technology. *Energies* **2022**, *15*, 1086. [CrossRef]
41. Bae, H.; Kim, Y. Technologies of lithium recycling from waste lithium ion batteries: A review. *Mater. Adv.* **2021**, *2*, 3234–3250. [CrossRef]
42. Kim, H.-J.; Krishna, T.; Zeb, K.; Rajangam, V.; Gopi, C.V.V.M.; Sambasivam, S.; Raghavendra, K.V.G.; Obaidat, I.M. A Comprehensive Review of Li-Ion Battery Materials and Their Recycling Techniques. *Electronics* **2020**, *9*, 1161. [CrossRef]
43. Beaudet, A.; Larouche, F.; Amouzegar, K.; Bouchard, P.; Zaghib, K. Key Challenges and Opportunities for Recycling Electric Vehicle Battery Materials. *Sustainability* **2020**, *12*, 5837. [CrossRef]
44. European Commission 2050 Long-Term Strategy. Available online: https://ec.europa.eu/clima/eu-action/climate-strategies-targets/2050-long-term-strategy_en (accessed on 3 May 2022).
45. Pražanová, A.; Míka, M.H.; Knap, V. Lithium-ion battery module-to-cell: Disassembly and material analysis.J. *Phys. Conf. Ser.* **2022**, *2382*, 12002. [CrossRef]
46. Meng, F.; Guo, H.; Wang, Z.; Yan, G.; Li, X. Modification by simultaneously γ-WO3/Li2WO4 composite coating and spinel-structure formation on Li[Li0.2Mn0.54Ni0.13Co0.13]O2 cathode via a simple wet process. *J. Alloys Compd.* **2019**, *790*, 421–432. [CrossRef]
47. Gan, Z.; Hu, G.; Peng, Z.; Cao, Y.; Tong, H.; Du, K. Surface modification of LiNi0.8Co0.1Mn0.1O2 by WO3 as a cathode material for LIB. *Appl. Surf. Sci.* **2019**, *481*, 1228–1238. [CrossRef]
48. Wang, Y.; Yin, C.; Song, Z.; Wang, Q.; Lan, Y.; Luo, J.; Bo, L.; Yue, Z.; Sun, F.; Li, X. Application of PVDF Organic Particles Coating on Polyethylene Separator for Lithium Ion Batteries. *Materials* **2019**, *12*, 3125. [CrossRef] [PubMed]

Disclaimer/Publisher's Note: The statements, opinions and data contained in all publications are solely those of the individual author(s) and contributor(s) and not of MDPI and/or the editor(s). MDPI and/or the editor(s) disclaim responsibility for any injury to people or property resulting from any ideas, methods, instructions or products referred to in the content.